Methyl Oleate Synthesis by TiO$_2$ Photocatalytic Esterification of Oleic Acid: Optimisation by Response Surface Quadratic Methodology, Reaction Kinetics and Thermodynamics

Rosilene A. Welter,*[a, b] Harrson Santana,[b] Lucimara G. de la Torre,[b] Mark Robertson,[a] Osvaldir Pereira Taranto,[b] and Michael Oelgemöller*[a, c]

Methyl oleate, an example of a FAME (fatty acid methyl ester), was produced by oleic acid (OA) photoesterification with TiO$_2$ and UVA light. Different parameters were evaluated and optimised: catalyst pretreatment, temperature (25–65 °C), catalyst loading (1–30% w/w$_{OA}$) and oleic acid:alcohol molar ratio (1:3–1:55). Response surface quadratic methodology obtained by central composite rotational design (RSM-CCRD) was used to evaluate the main operational conditions of the photoesterification process. A high conversion of 98% ($\pm$0.8) at 55 °C, 20%

TiO$_2$ (w/w$_{OA}$), and 1(OA):55(methanol) molar ratio was achieved. The photoesterification mechanism is furthermore proposed. The Langmuir-Hinshelwood kinetic model considered the forward and backward reaction as first-order fits with the best accuracy (R^2 of 0.997). The thermodynamic results ($\Delta G_{338.15K} = -20.75$ kJ/mol, $\Delta H = 13.75$ kJ/mol, and $\Delta S = 0.47$ kJ/mol.K) indicate that the operating conditions are important, both to supply the energy requirement of the reaction, but also to increase the miscibility of the reactants.

Introduction

Biodiesel has gained increased importance as a substitute for fossil fuel. As a result, global biodiesel production increased from 6 billion litres per year in 2005 to 46 billion litres per year in 2020.[1] Biodiesel has several advantages over petrodiesel, most importantly, it is four times easier to degrade[2] and emits 86% fewer greenhouse gases.[3] Biodiesel is preferentially obtained from renewable sources such as vegetable oils, and is frequently produced by transesterification catalysed by strong acids. However, the efficiency of biodiesel as a fuel source is commonly reduced due to its high free fatty acid (FFA) content,[4] its production cost is high due to the need of advanced process technologies, and the large volumes of

reagents and waste involved demand appropriate treatment[5] Esterification is another method of producing biodiesel because of the easy availability of raw materials with high free fatty acid content.[4–7] Vegetable oils, such as canola oil and waste cooking oil (WCO), contain a high amount of oleic acid.[8,9] The use of WCO causes an about 60% reduction in the cost of biodiesel production.[10] Thus, the esterification of free fatty acid represents a promising option for biodiesel production.

The esterification reaction of free fatty acid occurs preferably in the presence of short-chain alcohols (methanol, ethanol or propanol) and requires a catalyst.[7,11–14] The most common catalysts are strong acids such as sulfuric acid. However, the use of strong acids causes problems such as equipment corrosion, the necessary removal of the catalyst, and the large amounts of waste generated.[15] These issues may be circumvented by a solid eco-friendly catalyst and photochemical activation. Photocatalysis using metal oxide and light is generally used to degrade organic compounds.[16,17] However, this methodology is also promising for the esterification of free fatty acid.[16,17] For example, UVC light-irradiated ZnO/SiO$_2$ resulted in a conversion of 96% for free fatty acid from *Jatropha curcas*,[4] while Cr/SiO$_2$ in the presence of solar light gave a conversion of 96% for free fatty acid from waste cooking oil.[18] La^{3+}/ZnO–TiO$_2$ irradiated by UVC light produced a conversion of 96% for free fatty acid from waste cooking oil.[7] Clay-supported anisotropic Au-modified N, S-doped TiO$_2$ nanoparticles in the presence of UV-Vis showed a conversion of 87% for oleic acid.[19] The advantage of photoesterification is the often high conversion under mild operational conditions (temperature and pH), the high purity of the photoproduct, and the easy recovery and reuse of the photocatalyst. However,

[a] R. A. Welter, Dr. M. Robertson, Prof. Dr. M. Oelgemöller
     College of Science and Engineering
     James Cook University
     Townsville, Queensland 4811 (Australia)
     E-mail: lene.welter@gmail.com
[b] R. A. Welter, Dr. H. Santana, Prof. Dr. L. G. de la Torre, Prof. Dr. O. P. Taranto
     School of Chemical Engineering
     University of Campinas
     13083-852, Campinas, SP, (Brazil)
[c] Prof. Dr. M. Oelgemöller
     Faculty of Chemistry and Biology
     Hochschule Fresenius gGmbH-University of Applied Science
     Limburger Str. 2
     D-65510, Idstein (Germany)
     E-mail: michael.oelgemoeller@hs-fresenius.de

ChemPhotoChem

Research Articles
doi.org/10.1002/cptc.202200007

Chemistry Europe
European Chemical
Societies Publishing

photocatalysis frequently requires complex pretreatments to enhance FAME production.

Titanium dioxide is non-toxic, chemically stable, easy to handle, and recoverable.[20] Therefore, it has been used for the degradation of organic pollutants such as dyes, pesticides and pharmaceuticals.[21–23] In contrast, synthetic photocatalysis with TiO_2 has not been explored widely.[24] However, some authors successfully developed esterification protocols using titanium dioxide and light irradiation. For example, capric acid esterification in the presence of glycerol resulted in a conversion of 97%,[17] crude palm oil with methanol of 96%,[25] and oleic acid with methanol of 86%,[6] respectively. Despite these encouraging studies, the TiO_2-photoesterification process has not yet been optimised in terms of its operational conditions, synergic effects between reagents and catalyst, or catalyst reuse. The thermodynamic and kinetic reaction parameters have also not been established yet, and these parameters are crucial for the development of a scalable and cost-efficient process.

Scale-up of heterogeneous photocatalytic processes remains challenging due to significant photon and mass transfer limitations.[26] Continuous-flow conditions can generally improve the performances of photochemical transformations,[27] and have subsequently become widespread in synthetic photochemistry.[28] Recently, heterogeneous photocatalysis has been realized in an advanced meso-scale flow reactor.[29] Numbering-up of smaller reactors has furthermore been demonstrated for photocatalytic water treatment.[30] Continuous-flow operation thus represents a promising strategy for photocatalytic biodiesel production. In fact, microreactors have been previously proposed for biodiesel production[31] as they improve the crucial mass transfer between reagents.[32]

This study aimed to develop an optimised photoesterification protocol based on experimental, thermodynamic, and physicochemical parameters. TiO_2 activation by UVA light and oleic acid in the presence of different short-chain alcohols were chosen as model systems. In addition, catalyst pretreatment and recovery processes were investigated. Several operational conditions, such as the oleic acid:alcohol molar ratio, catalyst content, and temperature, were considered.
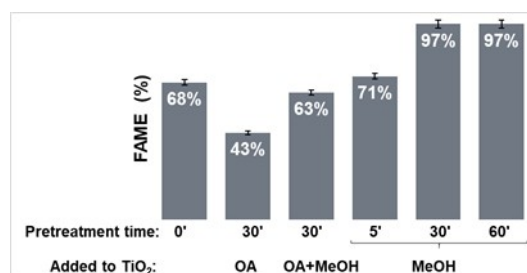
Figure 1. Oleic acid (OA) conversion (%) during photoesterification after different catalyst pretreatments: OA for 30 minutes, OA + MeOH for 30 minutes, and MeOH for 5, 30, and 60 minutes, respectively. Standard deviation < 1%. Photoesterification conditions: 55 °C, 1OA mol:55MeOH moles, 20% TiO_2 (w/w$_{OA}$).

Results and Discussion

Catalyst: TiO_2 nanoparticles

Photocatalyst pretreatment

The impact of reagent absorption (oleic acid and alcohol) on the photoesterification efficiency was initially studied by evaluating oleic acid conversion rates after each individual pretreatment. The addition of oleic acid was found to decrease the photocatalyst's efficiency (Figure 1), possibly due to the formation of a film on TiO_2 that blocked its pores.[33] Oleic acid may also reduce light access to the photocatalyst due to its higher refractive index compared to methanol (at 55 °C, RI_{OA}: 1.4475,[34] RI_{MeOH}: 1.3165[35]), especially at lower wavelengths such as UVA.[34] The initial addition of methanol prevents oleic acid from covering the surface of TiO_2, and 30 minutes of contact prior to the addition of oleic acid was found sufficient to fill the catalyst's interstices. According to the BET model constant value ($C_{BET} > 1$, Table 1), coverage occurred in a monolayer. The methanol monolayer adsorption arises through the binding of its oxygen atom with the TiO_2 (anatase). Additionally, a weak hydrogen bond from methanol to TiO_2 has been described, resulting in a monodentate configuration.[36] The monolayer configuration results in a higher adsorption energy (0.7–0.74 eV) than the second layer (0.24 eV). In contrast, methanol and rutile result in a stronger interaction than anatase but still form a monolayer.[37]
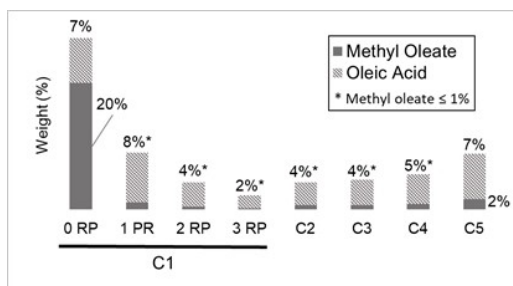
Table 1. TiO_2 characterisation by physisorption.					
	Pore vol. [cm³/g]	Pore diameter [nm]	Surface area [m²/g]	Particle size [nm]	C_{BET}
TiO_2 pure	0.74	3.52	51.851[a]	27.55	61.33
TiO_2 0 RP	0.61	3.03	37.57	38.03	26.63
TiO_2 C1	0.67	3.18	47.34	30.14	35.94
TiO_2 C5	0.62	3.02	41.20	34.67	29.01
[a] Surface area standard value according to the manufacturer: 35–65 m²/g.[39]					

Physicochemical characterisation of TiO₂

TiO$_2$ was characterised qualitatively and quantitatively before and after photoesterification, recovery, and reuse. According to the data obtained by FTIR-ATR and TGA/DSC after photoesterification (Figure 2 and S 3), the photocatalytic material retained 27% (w/w) of organic material (74% of FAME and 26% of oleic acid). FAME was removed easier than oleic acid during the recovery process, confirming that FAME adsorbed weaker than oleic acid. The complete recovery and washing process (3 RP) effectively removed 93% of organic material. The remaining 7% possibly consisted of oleic acid present in the internal interstices of the nanoparticles. After five complete cycles of photoesterification and subsequent recovery (C5), 9% (w/w) of organic material remained on TiO$_2$ (22% of FAME and 78% of oleic acid).

The physical characteristics of TiO$_2$ changed due to the presence of organic material, as shown in Table 1. Two effects were notable. The pores became obstructed, causing a reduction in pore volume and diameter, and a decrease in the catalyst surface area. In addition, the particles' agglomeration changed, causing their size to increase, hence reducing their surface area was observed. After photoesterification, the high organic material content resulted in the obstruction of pores (a decrease of 28% in the surface area compared with pure TiO$_2$) and agglomeration of particles (an increase of 38% of particle size compared with pure TiO$_2$). After C1 (Photoesterification + 3 RP; Figure 2), the pores were accessible (a decrease of 9% in the surface area and 70% of the surface recovered compared with pure TiO$_2$) with less agglomeration (an increase of 9% of particle size compared with pure TiO$_2$). After 5 cycles of catalyst use and recovery, the organic material was more impregnated; however, particles were almost open (a decrease of 11% in the surface area compared with pure TiO$_2$) but showed higher particles agglomeration (an increase of 26% of particle size compared with TiO$_2$).

RD analysis (Table 2, supplementary material section S 3) produced almost constant results for all samples. The crystallite size had an average of 21.65 nm ($\pm$0.65). The composition was 90% of anatase and 10% of rutile, similar to that obtained by EDS analysis (Figure 3d; supplementary material section S 3). The combination of different TiO$_2$ crystallite forms (anatase and rutile) improves the photocatalytic efficiency due to synergic effects. Consequently, the transfer of photo-excited electrons and positive holes in the crystallite forms can occur.[38]

SEM analyses (Figure 3a–c) showed variations in the catalyst's structure. After five cycles, the particles were slightly more agglomerated with sharper structures. This aggregation may block the active sites, reducing the catalytic activity and catalyst's stability.[38] In addition, the catalyst powder showed visible differences (Figure 3e). A higher content of organic matter resulted in a darker, heavier, and more clustered powder.
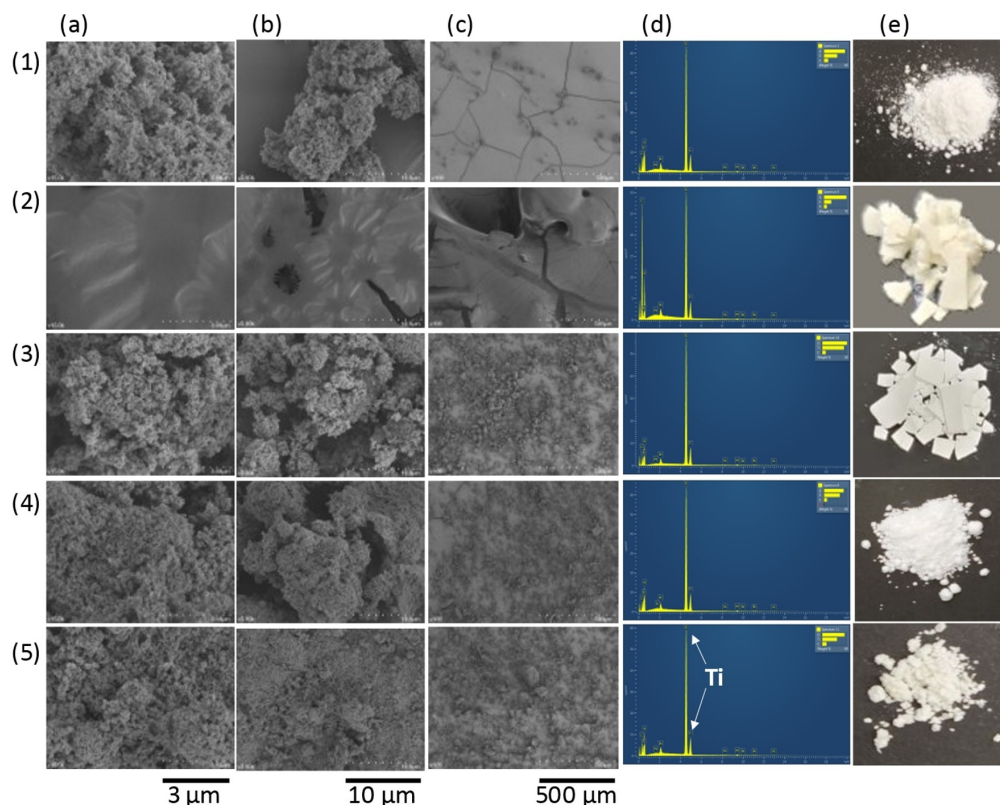
Photoesterification reactions

Esterifications of oleic acid and short-chain alcohols (using TiO$_2$ irradiated by UVA as a catalyst) were evaluated in a batch reactor. The following operational conditions were assessed: temperature, catalyst loading, oleic acid:alcohol molar ratio, and alcohol type.

A high oleic acid conversion of 98% was obtained with a 1OA:55MeOH molar ratio and 20% w/w$_{OA}$ at 55 °C after 4 hours of irradiation. In comparison with other literature studies (Table 3), this result demonstrates that TiO$_2$ without any further modification can effectively initiate photoesterification if pre-treatment is carefully evaluated first.

Optimisation study: alcohol and catalyst content

Initially, the effects of two process variables (oleic acid:methanol molar ratio and catalyst content) on oleic acid conversion using a CCR design was performed (as described in Table S1 – supplementary material), and the results are summarised in Figure 4 and Figure 5. A clear correlation between these variables and the reaction performance was observed. The best values obtained were close to the CCR design's highest level of the content of catalyst (20% w/wOA) and methanol (1OA:55Me), suggesting further improvement potential of the experimental design (Figure 6 and Figure 7). Oleic acid conversions between 12% and 98% were achieved, clearly showing the importance of these two variables. The tests were conducted in triplicates and the experimental standard deviation (1OA:12Me/15% TiO$_2$ and 1OA:55Me/20% TiO$_2$, as described in Table S1 – supplementary material) resulted in a value of $\pm$0.00786, indicating excellent reproducibility of the

Figure 2. Organic material present within TiO$_2$ after photoesterification under operational conditions PC2. Values obtained by TGA and FTIR analysis (more details in S3) considering 0 (0RP) to 3 (3RP) washing procedure for the first use (C1), and up to 5 cycles of catalyst use.

Table 2. TiO₂ characterisation by XRD.[a]			
	Crystallite size[d] (nm)	Anastase⁴ (%)	Rutile⁴ (%)
TiO₂ pure	22.25	91%	9%
TiO₂ PE[b]	21.95	91%	9%
TiO₂ C1[c]	20.58	91%	9%
TiO₂ C5	21.53	90%	10%

[a] XRD: spectra are shown in S 3. [b] TiO$_2$ after photoesterification reaction. [c] after 1 cycle of photoesterification and 3RP. [d] Obtained by the Scherrer equation (Equation 2).

Figure 3. (1) Pure. (2) After photoesterification by operational conditions PC1. (3) After photoesterification by operational conditions PC2. (4) After 1 use (C1). (5) After 5 cycles of catalyst use and recovery (C5). (a) SEM image: 3 μm. (b) SEM image: 10 μm. (c) SEM image: 500 μm. (d) EDS. (e) Photographic images.

Table 3. Oleic acid and methanol esterification obtained by different catalysts and operational conditions.

Catalyst	% [w/w$_{OA}$]	MeOH:1OA Molar ratio	T [°C]	Time [h]	FAME [%]	Ref.
TiO_2 + UVA	20	55	55	4	98	This study
Au/TiO_2 + Visible light	10	9	40	6	85	[19]
Biomass-based polymers	3	15	75	3	96	[40]
Fe_3O_4@PILPW	13	12	90	5	93	[41]
[HMIM]HSO_4	15	15	110	8	95	[42]
HZ zeolite/1.0/60	10	45	100	4	83	[43]
HZ zeolite/2.0/80	10	45	100	4	73	[43]
HZ zeolite/0.5/60	10	45	100	4	71	[43]
HZ zeolite	10	45	100	4	55	[43]
LO (lanthanum oxide)	10	5	100	7	63	[44]
M-MMT K10 acid	5	10	60	3	70	[45]
SLO/HZSM-5	10	5	100	7	100	[44]
SLO (sulphated lanthanum oxide)	10	5	100	7	98	[44]
SO_3-HM-ZSM-5-3	5	18	88	10	100	[46]
Sugarcane bagasse-SO_3H	0.1	20	50	24	85	[47]
TiO_2 + UVA	15	12	30	4	75	[6]
TiO_2/NP-800	10	8	150	8	87	[48]
TPA3/MCM-41	3.7	40	60	6	100	[49]
Zr(SO_4)$_2$	3	9	60	5	98	[50]
300-Nb_2O_5/SO_4^{2-}	5	20	100	4	92	[51]

experimental results. The elliptical contour of the response surface confirms that correlations between variables were significant[52] and the surface's shape reveals that the maximum efficiency for the process was obtained[53] (OA conversion of 97% (± 0.8%) for 20% (w/wOA) TiO_2 and 1OA:55MeOH). Further increase in the catalyst content (25% and 30% (w/wOA) TiO_2) produced a decrease in oleic acid conversion.

Based on the CCR design of the complementary tests (19 tests, as described in Table S1 – supplementary material), a mathematical model (Equation 1) was developed. The experimental and model data convergence resulted in an R^2 of 0.989 (Figure 8). According to ANOVA analysis (Table 4), it showed a p-value < 0.0001 and an F-value of 173.51 (F-value ≫ Fcrit).
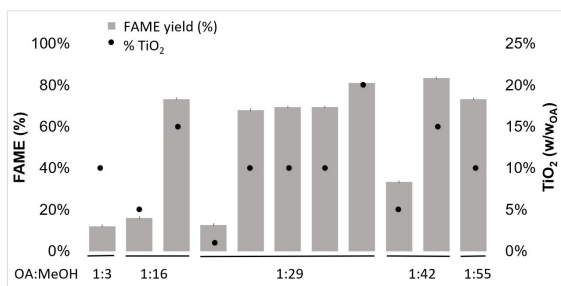
Figure 4. Central composite rotational (CCR) experimental design of oleic acid conversion (%) with methanol to FAME using TiO$_2$ and UVA irradiation: Oleic acid conversion (%) at equilibrium. Temperature: 55 °C, TiO$_2$ content range between 1% and 20% (w/w$_{OA}$) and OA : MeOH molar ratio range between: 1 : 3 and 1 : 55. Experimental standard deviation (σ) of ± 0.00786.
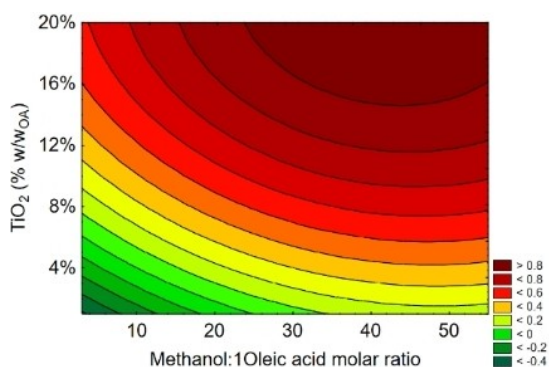
Figure 5. Central composite rotational (CCR) experimental design of oleic acid conversion (%) with methanol to FAME using TiO$_2$ and UVA irradiation: Surface response contour plots of FAME (%) conversion for catalyst content – oleic acid : methanol molar ratio. Temperature: 55 °C, TiO$_2$ content range between 1% and 20% (w/w$_{OA}$) and OA : MeOH molar ratio range between: 1 : 3 and 1 : 55. Experimental standard deviation (σ) of ± 0.00786.
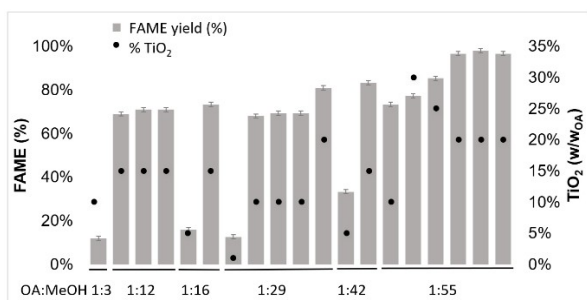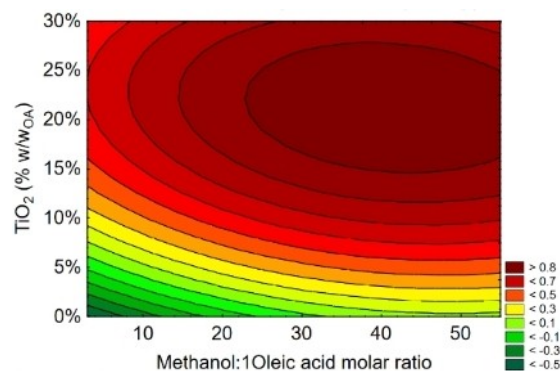

Figure 6. Central composite rotational (CCR) experimental design of oleic acid conversion (%) with methanol to FAME using TiO$_2$ and UVA irradiation: Oleic acid conversion (%) at equilibrium. Temperature: 55 °C, TiO$_2$ content range between 1% and 30% (w/w$_{OA}$) and OA : MeOH molar ratio range between: 1 : 3 and 1 : 55. Experimental standard deviation (σ) of ± 0.00786.

These parameters clearly reflect the accuracy between the mathematical model and the experimental results.

Figure 7. Central composite rotational (CCR) experimental design of oleic acid conversion (%) with methanol to FAME using TiO$_2$ and UVA irradiation: Surface response contour plots of oleic acid conversion (%) for catalyst content-oleic acid : methanol molar ratio. Temperature: 55 °C, TiO$_2$ content range between 1% and 30% (w/w$_{OA}$) and OA : MeOH molar ratio range between: 1 : 3 and 1 : 55. Experimental standard deviation (σ) of ± 0.00786.
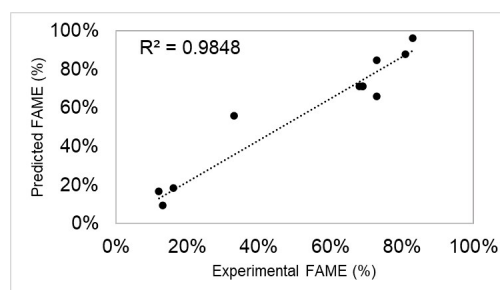
Figure 8. Oleic acid conversion (%) obtained by the model (Equation (1)) and experimentally (Figure 6). FAME produced by oleic acid and methanol photoesterification.

Table 4. ANOVA for RSM obtained by CCR design for two variables (TiO$_2$ (w/w$_{OA}$) and OA : MeOH molar ratio) for oleic acid and methanol photo-esterification.

	DF	SS	MS	F-value[a]	p-value
TiO$_2$	6	6066.27	1011.04	181.91	7.96E-5
OA : MeOH molar ratio	7	3052.07	436.01	78.45	4.07E-4
Model	13	12536.71	964.36	173.51	7.59E-5
Error	4	22.23	5.56		
Corrected total	17	12558.94			

[a]F$_{cricit}$: 4.49.

$$FAME\ (\%) = -0.5815 + 0.0283 \cdot 7(OA : MeOH) + 8.7801 \cdot (Cat) - 0.000291 \cdot (OA : MeOH)^2 - 0.0094 \cdot (OA : MeOH) \cdot (Cat) - 20.2811 \cdot (Cat)^2 \quad (1)$$

To understand the impact of catalyst loading and alcohol content separately, both were evaluated by the mathematical model obtained from RSM (Equation 1). The TiO$_2$ content showed a larger impact on FAME production than the OA : MeOH molar ratio. A high TiO$_2$ loading is required to increase the number of the active sites available by increasing the catalyst surface area, which was indeed observed until oleic

acid conversion peaked at 20% (w/w_{OA}) of TiO₂. However, values higher than 20% w/w_{OA} reduced oleic acid conversion. This reduction may be due to a decrease in the reaction medium's opacity and light scattering by the solid photocatalyst, hence reducing light incidence. Catalyst aggregation may have further reduced the catalyst surface area and hence photocatalytic efficiency. Despite the reaction stoichiometry of 1OA:1MeOH, a high alcohol concentration is needed to promote an efficient mix between the reactants.[54] A lower concentration of methanol, e.g., 1OA:12MeOH, resulted in an increased presence of oleic acid close to the catalyst, forming a film that blocks the pores and reduces light irradiation (Figure 3b). At high concentrations of methanol such as 1OA:55MeOH, the formation of these passivating films becomes less likely (Figure 3c).

The high photoesterification efficiency observed for methanol was not retained for other alcohols, i.e., ethanol and n-propanol (Table 5). This observation is in line with previous reports for other catalyst systems.[11,45,55] Methanol has a partial charge greater than ethanol or propanol and thus, it is a better electron donor for oleic acid esterification.[11] Consequently, the energy required to produce ethyl oleate or n-propyl oleate is higher than that of methyl oleate ($\Delta H^\circ_{methyl\ oleate} \ll \Delta H^\circ_{ethyl\ oleate}$, $\Delta H^\circ_{n\text{-propyl\ oleate}}$ and $\Delta c_{p,L}/R^2_{methyl\ oleate} \ll \Delta c_{p,L}/R^2_{ethyl\ oleate}$, $\Delta c_{p,L}/R^2_{propyl\ oleate}$).[7,11–14] The pronounced differences in photoesterification efficiencies observed for the three alcohols may also be caused by RI (refractive index) differences, with higher RIs lowering the catalyst's capacity, as described in section 2.1.1 (RI_{MeOH}: 1.3165, RI_{EtOH}: 1.3464, and RI_{n-PrOH}: 1.3704[35]).

Temperature relevance

The reaction temperature can have an impact on the reactants' miscibility and hence interfere with FAME yields. Temperature oscillations may also negatively impact on other operating conditions such as alcohol and catalyst content. Two distinct alcohol and catalyst loadings were thus investigated to evaluate the effect of temperature: PC1 (1:12 of OA:MeOH and 15% TiO₂ (w/w_{OA})) and PC2 (1:55 of OA:MeOH and 20% TiO₂ (w/w_{OA}). For each PC condition, 5 tests were carried out (range: 25°C to 65°C; supplementary material Table S1).

For both series, PC1 and PC2 operational conditions, higher conversions were obtained for higher temperatures (Figure 9). Between 25°C and 55°C, an almost constant increase was noted, while a plateau and thus reaction equilibrium was reached between 55°C and 65°C. According to the thermodynamic properties obtained from this study (section 2.5) and the
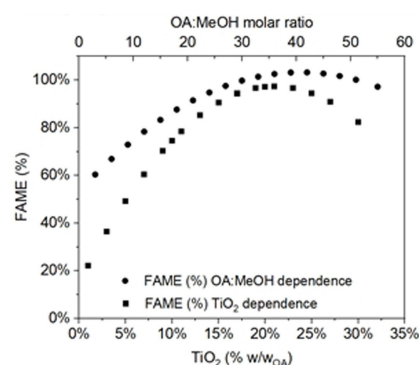

Figure 9. Predicted values of oleic acid conversion (%) considering % TiO₂ (w/w_{OA}) dependence (1OA:36MeOH molar ratio) and OA:MeOH molar ratio dependence (20% TiO₂ (w/w_{OA})), Temperature: 55°C.

literature,[11] temperature weakly influences the esterification reaction. However, a higher temperature is required to obtain miscibility between free fatty acid and the alcohol, considering that alcohol has a higher affinity to itself than free fatty acid molecules.[11,54,56] However, temperature alone is not sufficient to promote esterification. According to the blank tests (insert in Figure 10) the reaction requires a catalyst to achieve a better oleic acid conversion.

Relevance of individual operational conditions

The influence of the three independent variables (OA:MeOH, % TiO₂, and T) was analysed to understand their contribution to oleic acid conversion. A total of 33 experiments were performed (Table S1, including blank tests). According to these results (Table 6), the correlation between the variables is consistent (p-value < 0.0000 and an F-value of 27.891). Catalyst loading and temperature were identified as the more important variables (p-value < 0.0002), in agreement with the literature for related reactions.[57–61]
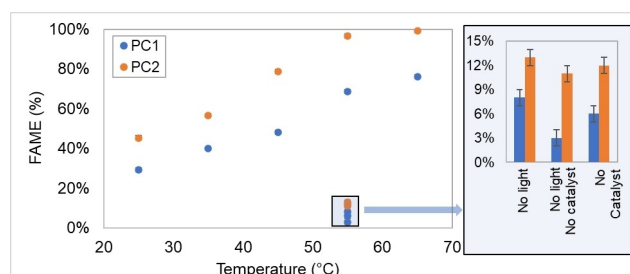
Figure 10. Oleic acid conversion (%) with methanol to FAME. Photoesterification temperature analysis by PC1 (15% TiO₂ (w/w_{OA}) and 1OA:12MeOH), and PC2 (20% TiO₂ (w/w_{OA}) and 1OA:55MeOH). PC1 and PC2 enlargement: Blank tests conducted at 55°C considering the absence of light (UVA), light and catalyst (TiO₂), and catalyst (TiO₂), respectively [(σ) of ±0.00786].

Table 5. Oleic acid esterification by different catalysts and alcohols.				
Catalyst	Methanol	Ethanol	n-Propanol	Ref.
M-MMT K10 acid	70	40	35	[45]
SnCl₂·2H₂O	77	68	36	[55]
TiO₂ + UVA[a]	97	21	6	This study
[a] Operational conditions: 55°C, 1OA:55Alcohol and 20% (w/w_{OA}) of TiO₂.				

ChemPhotoChem

Research Articles
doi.org/10.1002/cptc.202200007

Chemistry Europe
European Chemical
Societies Publishing

Table 6. Oleic acid conversion (%) according to the dependent variables: TiO_2 content, OA:MeOH molar ratio, and temperature.

	β^*	SD of β^*	β	SD of β	t (23)	p-value
Intercept			−55.5258	17.29893	−3.20978	0.003516
OA:MeOH	0.161204	0.104961	0.2514	0.16366	1.53585	0.136655
% TiO_2	0.745494	0.106086	2.9950	0.42619	7.02726	0.000000
T (°C)	0.413575	0.096892	1.2624	0.29576	4.26840	0.000232

$R^2 = 0.76$, $F_{(3,26)} = 27.891$, $p_{value} < 0.0000$, and SD = 15.052.

Photocatalyst reuse

The reuse of photocatalyst resulted in a drop in conversion of 21% when compared with its first usage (Figure 11). However, the conversion remained constant between subsequent reuse reactions (C2 to C5). This finding suggests a reduction in the exposed catalyst's active sites. Besides a decrease in the contact area, residual oleic acid formed a passivating film on the catalyst's surface, thus blocking its pores and reducing the penetration of light. The catalyst's analysis and characterisation (discussed in section 2.1.2) supports this interpretation. A decrease of pores and surface area was observed by N_2 physisorption and an increase of organic material impregnated on the catalyst was noted by FTIR and TGA. A similar behaviour was observed for Ni-doped ZnO nanocatalyst used for castor oil transesterification and its decrease in efficiency was associated with the deposition of organic material and a subsequent reduction in active sites.[7,62]

Moreover, reductions in catalytic efficiencies are commonly observed, as shown in Table 7. Nevertheless, the consistency in performances between 2 and 5 uses' cycles indicate that the catalyst retains its general stability and reactivity, thus making its reuse feasible and economical.
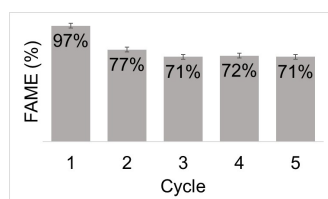
Figure 11. Catalyst reuse. Operational conditions PC2: 55 °C, 1OA mol:55MeOH mols, 20% TiO_2 (w/w$_{OA}$) [(σ) of ±0.00786].

Table 7. Catalyst reuse for oleic acid and methanol photoesterification.

| Catalyst	FAME [%]	# cycles	FAME [%]	Decrease [%][a]	Ref.
TiO_2 + UVA	98	5	71	28	This study
Fe_3O_4@PILPW	93	6	90	3	[41]
HPA/ZIF(His.)	92	4	73	18	[66]
LO (lanthanum oxide)	63	3	10	84	[44]
SLO/HZSM-5	100	3	52	48	[44]
SLO (sulphated lanthanum oxide)	98	3	28	71	[44]
TiO_2/NP-800	87	6	70	20	[48]
$Zr(SO_4)_2$	98	4	41	57	[50]

[a] Decrease between first and last cycle.

Photoesterification reaction mechanism

The accepted mechanism for oleic acid photoesterification with methanol in the presence of TiO_2 is depicted in Scheme 1.[7,63] TiO_2 excitation by photons (h^+) with sufficient energy to overcome its bandgap causes charge separation (Step 1).[6,64] Electrons (e^-) are promoted to the conduction band (CB), generating positive holes (h^+) in the valence band (VB).[65] Both species (h^+ and e^-) subsequently react with methanol (step 2) and oleic acid (step 3) adsorbed on the catalyst's surface. The hole (h^+) accepts an electron from the hydroxy-group, generating a methoxy radical ($CH_3O^\bullet$), while the electron (e^-) in the conduction band reacts with oleic acid, creating a carboxyl radical anion ($RCO_2^{-\bullet}$). Both reactive intermediates combine and, after further reaction steps, form the ester and water (step 4). Alternative mechanisms have also been proposed.[6,17]
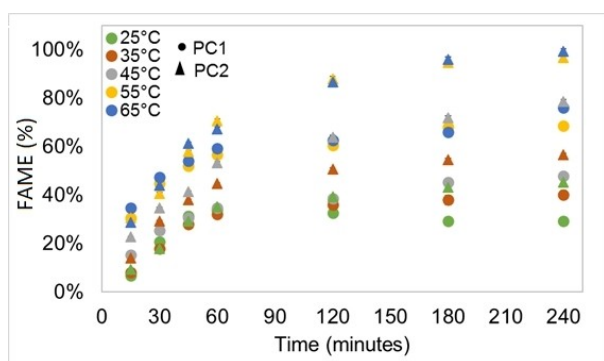
Kinetics properties

Kinetic curves were obtained for all experiments, and a reaction time of 4 hours was found sufficient to reach equilibrium. For
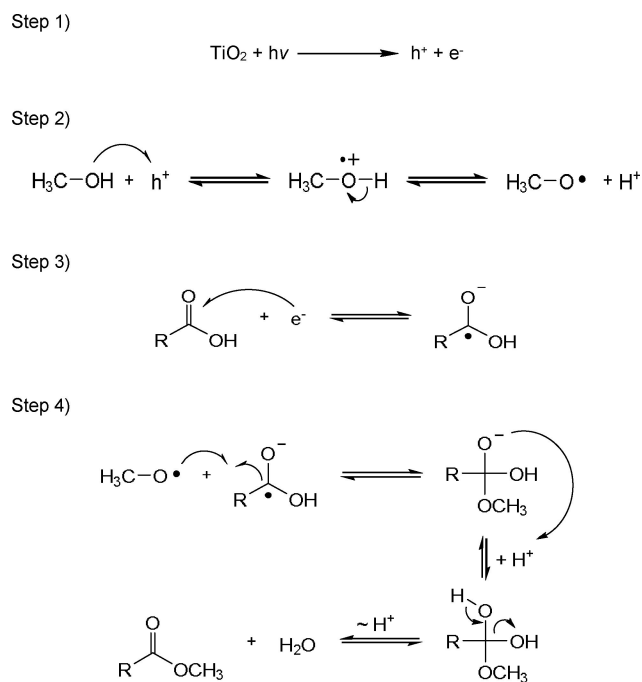
Scheme 1. Accepted photoesterification mechanism for oleic acid and methanol (R = cis-$CH_3(CH_2)_7CH=CH(CH_2)_7$).

mathematical modelling, kinetic and equilibrium data obtained for PC1 (1OA mol:12MeOH mols, 15% TiO_2 (w/w$_{OA}$)), and PC2 (1OA mol:55MeOH mols, 20% TiO_2 (w/w$_{OA}$)) within a temperature range of 25–65°C were considered. The kinetic results for photoesterification are shown in Figure 12. At low temperatures (25 and 35°C) and methanol content (1OA:12MeOH of PC1), mixing is not efficient and after the first hour, reductions in conversions were observed. In particular, inefficient reagent ratios in combination with the hygroscopic nature of TiO_2 may favour water retention at the catalyst, thus favouring hydrolysis. At low temperature and high methanol content (all temperatures evaluated for 1OA:55MeOH - PC2, Figure 12), or at high temperature and low methanol content (45, 55, and 65°C for
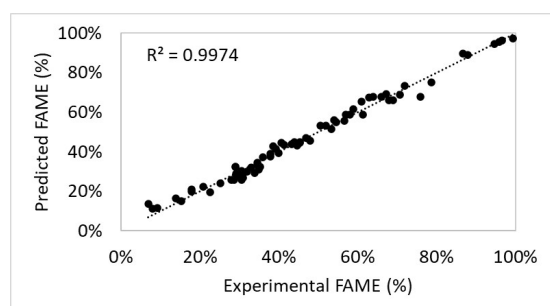
1OA:12MeOH - PC1, Figure 12) hydrolysis was successfully supressed. Hence, high temperatures and methanol contents are desirable to achieve a high esterification efficiency. Based on these overall findings, the kinetic mathematical model may result in a better accuracy when considering the backward reaction (hydrolysis). Five kinetic models were subsequently evaluated (Equation 7–10, Table 11, section 4.5), and their statistical analysis is shown in Table 8. The Langmuir-Hinshelwood (L-H) model achieved the best agreement with the experimental data (Figure 13). This result highlights the importance of evaluating the heterogeneous catalytic reaction through models that consider the presence of active sites.

The L-H kinetic model was subsequently used to obtain kinetic parameters for PC1 and PC2 operational conditions at different temperatures (Figure 14a). k_1 (esterification) and k_{-1} (hydrolysis) resulted in a $K_{eq} < 1$ for low temperatures and $K_{eq} > 1$ for high temperatures (Figure 15). This confirms that the hydrolysis reaction is significant for the low-temperature process, but not dominant for high methanol content. However, a higher methanol content improves the esterification

Figure 12. Oleic acid and methanol photoesterification kinetic curves. Catalyst: TiO_2 irradiated by UVA. PC1 (1OA mol:12MeOH mols, 15% TiO_2 (w/w$_{OA}$)) and PC2 (1OA mol:55MeOH mols, 20% TiO_2 (w/w$_{OA}$)).

Table 8. Kinetic models[a] statistical analysis applied to experimental kinetic data of oleic acid and methanol photoesterification.[b]

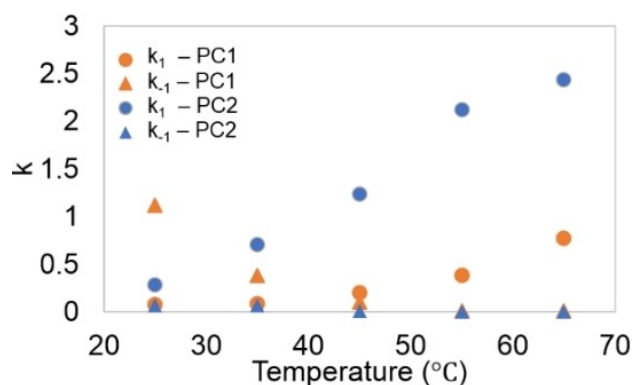| Model[a,b]	R^2	SD	p-value	F-test
HSE1HN	0.928	0.066	< 0.0000	877.551
HSE1H1	0.939	0.061	< 0.0000	1047.042
HSE1H2	0.931	0.065	< 0.0000	1008.048
HSE2H2	0.480	0.122	< 0.0000	62.878
L-H	0.997	0.026	< 0.0000	4726.083

[a] Equation 7-10 (Table 11). [b]Kinetic data evaluated at time: 15, 30, 45, 60, 120, 180, and 240 minutes. For PC1 (1OA mol:12MeOH mols, 15% TiO_2 (w/w$_{OA}$) and PC2 (1OA mol:55MeOH mols, 20% TiO_2 (w/w$_{OA}$)).

Figure 14. Kinetic constants for the forward reaction (esterification, k_1) and for the backward reaction (hydrolysis, k_{-1}), obtained by the L-H kinetic model (Equation 11). Two operational conditions were evaluated: PC1 (1OA mol:12MeOH mols, 15% TiO_2 (w/w$_{OA}$) and PC2 (1OA mol:55MeOH mols, 20% TiO_2 (w/w$_{OA}$)).
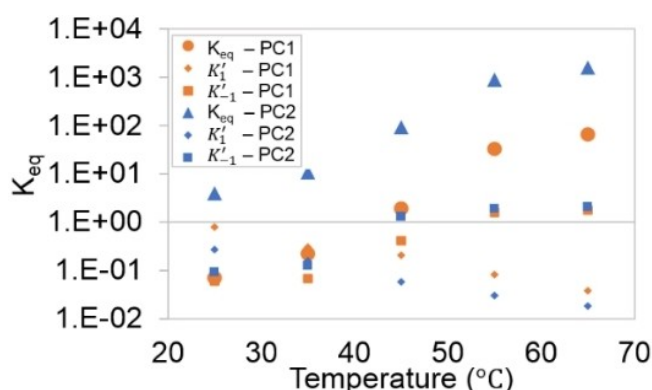

Figure 13. Experimental and modelling data obtained by L-H kinetic model (Equation 11, Table 11) for FAME (x_{FAME}) obtained by oleic acid and methanol photoesterification. The x_{FAME} was evaluated at t: 15, 30, 45, 60, 120, 180 and 240 minutes for PC1 (1OA mol:12MeOH mols, 15% TiO_2 (w/w$_{OA}$)) and PC2 (1OA mol:55MeOH mols, 20% TiO_2 (w/w$_{OA}$)).

Figure 15. Equilibrium constant for esterification/hydrolysis reaction (K_{eq}), equilibrium constant for oleic acid adsorption on active catalyst site (K'_1), and equilibrium constant for FAME adsorption on active catalyst site (K'_{-1}). Two operational conditions were evaluated: PC1 (1OA mol:12MeOH mols, 15% TiO_2 (w/w$_{OA}$) and PC2 (1OA mol:55MeOH mols, 20% TiO_2 (w/w$_{OA}$)).

ChemPhotoChem

Research Articles
doi.org/10.1002/cptc.202200007

**Chemistry
Europe**
European Chemical
Societies Publishing

reaction according to K_{eq} (1OA:55MeOH molar ratio) $\gg K_{eq}$ (1OA:12MeOH molar ratio). K'_1 and K'_{-1} refer to oleic acid and FAME adsorption on the catalyst's active sites, respectively. According to the increase in reaction efficiency, K'_1 decreased and K'_{-1} increased, which indicates that oleic acid and FAME compete for adsorption on the catalyst. However, $K_{eq} \gg K'_1$ and K'_{-1} reveals that the reagent adsorption on the catalyst does not limit the reaction and it instead maintains its catalytic capacity. Moreover, the parameter (K) variation in the photochemical process suggests that the reaction does not have a rate-determining 'light-intensity limited' step.[65] Thus, the energy from the catalyst's charge separation is enough to drive the reaction sufficiently.
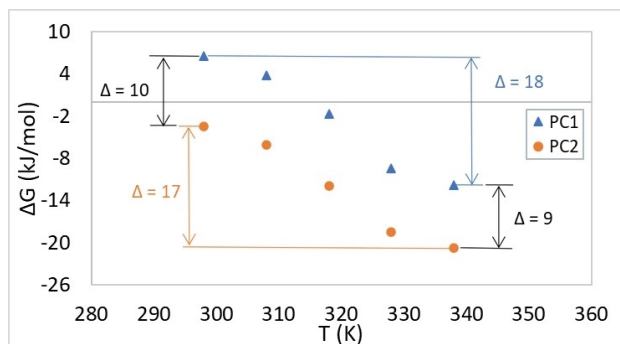
Thermodynamic properties

The thermodynamic properties of the oleic acid photoesterification with methanol were likewise determined. The Arrhenius and van't Hoff models (Equation 4 and Equation 5, details in S 5) were used to obtain E_a, A, ΔH, and ΔS (Table 9). The energy required for operational conditions PC2 is lower than PC1, confirming that methanol content and temperature are significant parameters for improving the photoesterification efficiency. ΔH was determined as 15.61 kJ/mol for the 1OA:12MeOH and 13.75 kJ/mol for the 1OA:55MeOH molar ratio, respectively. This slight difference shows that a high methanol amount is predominantly required to mix the reagents. ΔH of the oleic acid/methanol photoesterification

depends on each process analysed and according to the literature, it is possible to obtain values between 7 and 50 kJ/mol.[11,67–69]

Furthermore, the positive values of ΔH and ΔS demonstrate that the reaction requires high temperatures. The ΔG (Equation 6) behaviour is shown in Figure 16. High temperatures and methanol content result in lower ΔG, favouring the esterification reaction. However, the methanol content ($\Delta G \approx 10$ kJ/mol) interferes less than temperature ($\Delta G \approx 17$ kJ/mol). Due to the positive value of ΔH and the negative value of ΔG, ΔS is a significant thermodynamic parameter, as known from the literature.[68] Therefore, the reagents' miscibility is relevant as maintained by a high content of methanol and/or a higher disorder caused by temperature increments. This behaviour supports literature findings,[11,54] where high alcohol contents and temperatures were required to mix the reagents properly and to achieve high esterification efficiencies. The Gibbs energy also reflects the catalyst behaviour, considering that after photoexcitation, the process is spontaneous ($\Delta G < 0$), mainly because of the exothermic natures of step 3 ($\Delta G_e < 0$) and step 4 ($\Delta G_h < 0$) in Scheme 1.[65] The $\Delta G < 0$ may result from systems where the reduction and oxidation steps do not need to be spatially or chemically separated.[65]

Conclusions

An optimised photoesterification process using TiO_2 and UVA irradiation with high efficiency to produce methyl oleate from oleic acid (conversion: 98%) was developed. Optimal conditions were obtained after catalyst pretreatment and with a loading of 20% wt/wt_{OA} and an oleic acid:alcohol molar ratio of 1:55 at 55 °C. The catalyst was reusable, proving its efficiency even after five cycles (FAME > 70%). Kinetics modelling was carried out and thermodynamic properties were obtained. According to these, a temperature higher than 55 °C and excess of alcohol are required to reach a high conversion rate. Low temperatures and/or lower alcohol contents result in reduced conversions and/or reverse reactions (hydrolysis). The simple optimised process obtained in this study overcomes the difficulties frequently observed for FAME production by oleic acid esterification using thermal methods (high temperature, extreme pH, difficult catalyst reuse and recovery, large volumes of water, complex FAME purification). Future research will investigate potential applications of the developed process to produce biodiesel from other free fatty acids, crude oils and waste cooking oil, as well as solar operation[70] and process scale-up.

Table 9. Thermodynamic properties for photoesterification obtained by PC1 and PC2 operational conditions at a temperature range between 25 °C and 65 °C by kinetic parameters obtained by the L-H kinetic model.

	PC1[a]		PC2[b]	
	Esterification	Hydrolysis	Esterification	Hydrolysis
E_a (kJ/mol)	5.033	−0.153	4.583	−0.133
A (min⁻¹)	4.02E+07	3.78E-19	3.91E+07	9.65E-18
ΔH (kJ/mol)	15.609		13.748	
ΔS (kJ/mol.K)	0.498		0.471	

[a] PC1: 1OA mol:12MeOH mols, 15% TiO_2 (w/w_{OA}). [b] PC2: 1OA mol:55MeOH mols, 20% TiO_2 (w/w_{OA}).

Figure 16. Gibbs energy variation for oleic acid and methanol photoesterification. PC1: 1OA mol:12MeOH mols, 15% TiO_2 (w/w_{OA}). PC2: 1OA mol:55MeOH mols, 20% TiO_2 (w/w_{OA}).

Methodology

Materials

Reagents and solvents were obtained from the following suppliers: TiO_2 (P25: Aeroxide®, Evonik), methanol (HPLC grade, Fisher Chemical), oleic acid 90% (Sigma-Aldrich), dichloromethane

ChemPhotoChem

Research Articles
doi.org/10.1002/cptc.202200007

Chemistry
Europe
European Chemical
Societies Publishing

(DCM, AR, 99.5%, Univar), sodium hydroxide pellets (NaOH, Univar), acetone (AR, 99.5%, ChemSupply), diethyl ether (AR, 99.5%, Univar), ethanol (AR, 99.5%, Univar), 0.02 N potassium hydroxide in aqueous solution (KOH$_{aqueous}$, ±0.5%, Ace Chemical Company), 0.02 N potassium hydroxide in ethanol solution (KOH$_{ethanol}$, ±0.5%, Ace Chemical Company) and n-propanol (AR, 99.5%, ChemSupply). Samples were filtered through a Hydraflon 0.22 μm, 35 mm syringe filter. Irradiations were conducted in a Rayonet RPR-200 photochemical reactor (Southern New England Ultraviolet Company) equipped with 16 F8T5/BL fluorescent tubes (Ushio, 8 W Black Light UVA T-5 G5 Base). NMR spectra were recorded on a Bruker Ascend^{TM} 400 MHz Spectrometer. Fourier transform infrared spectroscopy-Attenuated total reflectance (FTIR-ATR) was carried out using a Nicolet™ iS™ 5 FTIR Spectrometer, coupled with an iD7 ATR accessory (ThermoFisher Scientific). Particle analyses were conducted using the Quantacrome AsiQwin equipment. The surface morphology was analysed by scanning electron microscopy (SEM, JSM-5410LV SEM-EDS Oxford). Elemental chemical characterisation was obtained by energy dispersive spectrometer (EDS), using a JSM-5410LV SEM-EDS Oxford.

TiO$_2$ Catalyst

Pretreatment

TiO$_2$ was mixed with the reactants for a specific time before starting the photoreaction. Five tests were conducted: (1) OA (30 minutes), (2) OA + MeOH (30 minutes), (3) MeOH (5 minutes), (4) MeOH (30 minutes), and (5) MeOH (60 minutes) (supplementary material, Table S1). The catalyst was mixed with the respective reagent by magnetic stirring (300 rpm) at 55 °C, the same temperature used in the following photoesterification tests. Catalyst and reactant were added according to the correct weight necessary for the reaction (supplementary material, Table S1). After pretreatment, the mixture (catalyst and reactant) was loaded into the reactor prior to photoesterification. The subsequent photoesterification experiments occurred at constant operational conditions, as indicated in section 4.3.1.

Recovery and reuse

At the end of each photoesterification experiment, the catalyst was filtered, washed with acetone (mixing vigorously with magnetic stirring at 500 rpm), allowed to settle for 20 hours, and the acetone layer was removed by decantation (1RP). After three repetitions (3RP), the catalyst was dried at 100 °C for 24 hours, crushed, and stored in a plastic vial at room temperature. The efficiency and reusability of the recovered TiO$_2$ were evaluated by characterisation and subsequent photoesterification tests. The photoesterification test followed by 3RP was considered as one complete cycle of catalyst reuse (C1). This process was performed five times (C1, C2, C3, C4, and C5) as tests 39 to 43, described in Table S1.

Characterisation

TiO$_2$ characterisation analyses prior and after each photoesterification were performed as follows: chemical characterisation was conducted by FTIR-ATR at room temperature in the spectral range of 400–1000 cm^{-1}. Spectra analysis was carried out using OriginPro 2021® (Learning Edition, OriginLab Corporation). Peak deconvolution analysis was performed by PeakDeconvolution.opx from OriginLab® using the baseline model: Straight Line, Peak Resolution Enhancement Method: 2nd derivative Smooth Derivative Method: Quadratic Savitzki-Golay, 2nd order polynomial. Particle size, pores' volume, pore size, and total surface area were obtained by N$_2$ physisorption to perform isotherms: Brunauer, Emmet, and Teller (BET), and Barrett, Joyner and Halenda (BJH).[71] Thermoanalyses were carried out to determine the presence of organic material inside the catalyst's pores. Thermal gravimetric analysis (TGA) and differential scanning calorimetric (DSC) were performed by adopting air and nitrogen at 10 °C/min in a range of room temperature to 800 °C. The SDT650 equipment was used, and the data was handled by Trios® software (TA instruments) and OriginPro 2021® (Learning Edition, OriginLab Corporation). Crystalline material characterisation was conducted by X-ray powder diffraction (XRD) using a Siemens D5000 Diffractometer under the irradiation of Cu K α ($λ_{XRD}$ = 0.154060 nm). Spectra analysis was carried out using OriginPro 2021® (Learning Edition, OriginLab Corporation). The average crystallite size was obtained by the Scherrer equation (Equation (2)), using K$_{XRD}$ = 0.9 and $λ_{XRD}$ = 1.5406 Å, and considering the prominent peaks observed in the spectrum for anatase (25.23°) and rutile (27.43°).

$$D_C = \frac{K_{XRD} \cdot λ_{XRD}}{β_{XRD} \cdot \cos θ_{XRD}} \quad (2)$$

Photoesterification process

Photocatalytic esterification of oleic acid with methanol

TiO$_2$ was added to methanol and mixed at the respective photoesterification test temperature. After 30 minutes, TiO$_2$ + methanol and oleic acid were loaded into the reactor (Figure 17). The photoreactor and the reaction heating (water bath) were turned on 30 minutes prior to the photoesterification experiment. The cylindrical batch reaction vessel (100 mL) was manufactured of Pyrex glass (cut-off wavelength ≤ 290 nm) and was equipped with an inner 'cold' finger for heating. The reagents were mixed by magnetic stirring, and the reaction was stopped after 240 minutes. During kinetic studies, samples (<3 mL each) were withdrawn after set reaction times (15, 30, 45, 60, 120, 180, and 240 minutes). The samples were filtered by syringe, rota-evaporated at 40 °C to remove the liquid phase (170 mbar for 15 minutes, 72 mbar for 30 minutes, and 30 mbar for 30 minutes), and the conversion was determined by ^{1}H-NMR spectroscopy based on the integration of baseline separated signals. The final sample taken after 240 minutes was furthermore characterised (section 4.3.2) and stored in a glass vial at room temperature.
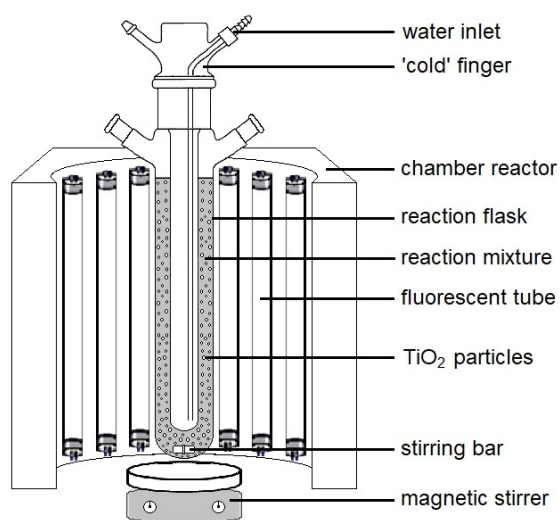
ChemPhotoChem

Research Articles
doi.org/10.1002/cptc.202200007

Chemistry Europe
European Chemical
Societies Publishing

Figure 17. Photoesterification reactor scheme.

Oleic acid conversion determination

Oleic acid conversions were determined by ^{1}H-NMR spectroscopy by correlating baseline separated FAME and oleic acid peak areas (supplementary material, Figure S4). The peak areas A_1 (CH_3O) and A_2 ($CH=CH$) were obtained using MestReNova® software (Version 6.0.2-5476, Mestrelab Research S.L.) and were used to determine the conversion rate as described in Equation (3).

$$\text{OA conversion (\%)} = 100 \cdot \left(\frac{A_2}{3} \cdot \frac{2}{A_1} \right) \qquad (3)$$

FTIR-ATR was alternatively used to determine oleic acid conversion rates (Details described in S3). Peak deconvolution analysis was carried out using PeakDeconvolution.opx (Origin-Lab®) by baseline model: Straight Line, Peak Resolution Enhancement Method: 2nd derivative Smooth Derivative Method: Quadratic Savitzki-Golay, 2nd order polynomial. The oleic acid conversion values were in agreement with those determined by NMR analysis.

Activation energies and enthalpies were determined using the Arrhenius (Equation (4)) and van't Hoff's (Equation (5)) models.

$$\text{Arrhenius model}: \ \ln(k) = -\frac{\Delta E}{R \cdot T} + \ln(A) \qquad (4)$$

$$\text{van't Hoff's model}: \ \ln(K) = -\frac{\Delta H}{R \cdot T} + \frac{\Delta S}{R} \qquad (5)$$

Optimisation study

The operational conditions (OA:MeOH molar ratio, TiO_2 loading and temperature) for photoesterification were evaluated to obtain an optimised reaction protocol. The Central Composite Rotational Design (CCRD) model for experimental development was followed, and the parameters' effects were analysed by response surface quadratic methodology (RSM), both obtained through Statistica 7.0® software.

A total of 33 experiments were carried out. The CCR design for two independent variables (OA:MeOH molar ratio and catalyst loading) was investigated using 11 experiments (Table 10, Entries 6 to 16 described in Table S1). Three additional tests were conducted as a triplicate using operation conditions extracted from the literature (Entries 17 to 19 in Table S1 with 1OA:12MeOH molar ratio and 15% w/w$_{OA}$ of TiO_2).[6] Two further test reactions were performed to extrapolate the CCRD model conditions (Entries 20 and 21 in Table S1 with 1OA:55MeOH molar ratio, 25% and 30% w/w$_{OA}$ of catalyst). Three experiments were conducted to confirm the best operational conditions (Entries 22 to 24, Table S1, triplicate of 1OA:55MeOH molar ratio and 20% w/w$_{OA}$ of TiO_2). Two more experimental tests were subsequently conducted to validate the mathematical model obtained (Entries 25 and 26 in Table S1). Three blank tests were furthermore performed by keeping the operational conditions constant (55°C, OA:MeOH as 1:55 and 20% of TiO_2 (w/w$_{OA}$)): Blank 1 (without catalyst), Blank 2 (without light with the reactor wrapped in aluminium foil), and Blank 3 (without catalyst and light with the reactor wrapped in aluminium foil) (Entries 27 to 29 in Table S1). The medium deviation was evaluated in triplicate (OA:MeOH as 1:29 and 10% of TiO_2 (w/w$_{OA}$), OA:MeOH as 1:12 and 15% of TiO_2 (w/w$_{OA}$), and OA:MeOH as 1:55 and 20% of TiO_2 (w/w$_{OA}$)).

RSM was used to investigate the operational conditions' relationship and their impact on FAME yields. A second-order polynomial order was used for the independent variables' interactions, and the oleic acid conversion was chosen as the response. The results were evaluated by the coefficient of determination (R^2), standard deviation (SD), occasionality of the results by null hypothesis (p-value), and experimental data adaptability to the model (F-test). In addition, the influence of each individual variable was analysed by their correlation with the dependent variables (unstandardised β* and standardised β), their significance (t-test), and their capacity to predict the dependent variable (p-level).

The temperature influence was investigated through 12 experiments (Entries 29 to 38 in Table S1). The temperatures selected were 25°C, 35°C, 45°C, 55°C, and 65°C, respectively. Two specific operational conditions were evaluated: (PC1), as described in the literature (1:12 of OA:MeOH and 15% TiO_2 (w/w$_{OA}$))[6] and (PC2), as obtained through this study (1:55 of OA:MeOH and 20% TiO_2 (w/w$_{OA}$)).

Moreover, the use of different alcohols (ethanol and n-propanol) was investigated by performing two experiments

Table 10. Operation parameters for oleic acid photoesterification optimisation by CCR design.

Parameter	Unit	Factorial and centre level			Axial level	
		Low (−1)	Centre (0)	High (+1)	Lowest (−√2)	Highest (√2)
OA:MeOH	molar ratio	1:16	1:29	1:42	1:3	1:55
Catalyst	(% w/w$_{OA}$)	5	10	15	1	20

ChemPhotoChem

Research Articles
doi.org/10.1002/cptc.202200007

Chemistry Europe
European Chemical
Societies Publishing

Table 11. Kinetic models evaluated for oleic acid and methanol photoesterification, experimental kinetic data (Equations (7)–(11)).

system	Assumptions	Model	Equation
Homogeneous	HSE1HN Forward reaction: first order Backward reaction: neglected	$\frac{dx_{FFA}}{dt} = -k_1 \cdot x_{FFA}$	(7)
	HSE1H1 Forward reaction: first order Backward reaction: first order	$\frac{dx_{FFA}}{dt} = k_{-1} \cdot (1 - x_{FFA}) - k_1 \cdot x_{FFA}$	(8)
	HSE1H2 Forward reaction: pseudo-first order Backward reaction: second order	$\frac{dx_{FFA}}{dt} = k_{-1} \cdot (1 - x_{FFA}) - k_1 \cdot C_{FFA_0} \cdot x_{FFA}^2$	(9)
	HSE2H2 Forward reaction: second order Backward reaction: second order	$\frac{dx_{FFA}}{dt} = k_{-1} \cdot C_{FFA_0} \cdot (1 - x_{FFA})^2 - k_1 \cdot C_{FFA_0} \cdot x_{FFA}^2$	(10)
Heterogeneous	L-H kinetic model[a] Forward reaction: first order Backward reaction: first order FFA and FAME are bounding the catalyst capacity	$\frac{dx_{FFA}}{dt} = k_{-1} \cdot \frac{K_2' \cdot x_{FFA}}{1 + K_2' \cdot C_{FFA_0} \cdot x_{FFA}} - k_1 \cdot \frac{K_1' \cdot (1 - x_{FFA})}{1 + K_1' \cdot C_{FFA_0} \cdot (1 - x_{FFA})}$	(11)

[a]Model's detailed development can be found in supplementary material - section S2.

(Entries 44 and 45 in Table S1), keeping the operational conditions constant (55 °C, OA:MeOH as 1:55 and 20% of TiO_2 (w/w$_{OA}$)).

Kinetics and thermodynamic parameters

Kinetic parameters are essential to understanding the reaction's performance over time, and by that, equilibrium conditions can be reached. Furthermore, future process scale-up modelling and simulations depend on these data to achieve reliable and applicable results. The equilibrium's composition is required to determine the equilibrium constant and the thermodynamic properties. Ten experimental kinetics were evaluated at different temperatures (range between 25 °C to 65 °C) and under two operational conditions (PC1 and PC2) (Entries 29 to 38 in Table S1). Five kinetics models, along with the reaction conditions proposed, were evaluated, as described in Table 11. Four models considered a homogeneous system with complete miscibility between reagents, and mass transfer effects were neglected. The difference between them is the order of the forward (esterification) and the backward reaction (hydrolysis). Based on literature findings, free fatty acid esterification by heterogeneous catalysis was satisfactorily described by the HSE1HN,[45] HSE1H2,[57] and HSE2H2,[66,72] HSE1H2,[73] and HSE2H2 models,[74,75] respectively. The Langmuir-Hinshelwood (L-H) kinetic model was chosen as the fifth model that considers a heterogeneous system with complete miscibility between reagents and a heterogeneous catalyst with active homogeneous sites. The L-H model is frequently used for photocatalysis with nanoparticles.[17,76–83]

Mathematical modelling was performed using the Matlab® software package and the results were evaluated by R^2, SD, p-value, and F-test. The parameters from the model with the best accuracy were subsequently used to obtain the thermodynamic properties. Using the Arrhenius model (Equation (4)), the temperature (T) effect was evaluated to obtain the activation energy (ΔE_a) and frequency factor (A). By the van't Hoff's model (Equation (5)), enthalpy (ΔH) and entropy (ΔS) were determined. Using Equation (6), the Gibb's free energy variation (ΔG) was obtained, which depended on T and an equilibrium constant (K_{eq}).

$$\Delta G = -R \cdot T \cdot \ln(K_{eq}) \tag{6}$$

Conflict of Interest

The authors declare no conflict of interest.

Data Availability Statement

Data sharing is not applicable to this article as no new data were created or analyzed in this study.

[1] O. Ogunkunle, N. A. Ahmed, *Energy Rep.* **2019**, *5*, 1560–1579.
[2] A. Demirbaş, *Energ. Source. Part A* **2008**, *31*, 169–174.
[3] E. Voegele, *Biodiesel Mag.* **2020**, *11*..
[4] G. Corro, U. Pal, N. Tellez, *Appl. Catal. B* **2013**, *129*, 39–47.
[5] B. Zhen, H. Li, Q. Jiao, Y. Li, Q. Wu, Y. Zhang, *Ind. Eng. Chem. Res.* **2012**, *51*, 10374–10380.
[6] M. C. Manique, A. P. Silva, A. K. Alves, C. P. Bergmann, *J. Mater. Sci. Eng. B* **2016**, *206*, 17–21.
[7] M. Guo, W. Jiang, C. Chen, S. Qu, J. Lu, W. Yi, J. Ding, *Energy Convers. Manage.* **2021**, *229*, 113745.
[8] M. Anwar, *Fuel* **2021**, *283*, 119204.

ChemPhotoChem

Research Articles
doi.org/10.1002/cptc.202200007

Chemistry Europe
European Chemical
Societies Publishing

[9] S. M. Ghazani, G. García-Llatas, A. G. Marangoni, *Eur. J. Lipid Sci. Technol.* **2014**, *116*, 380–387.

[10] M. Mohadesi, B. Aghel, M. Maleki, A. Ansari, *Renewable Energy* **2019**, *136*, 677–682.

[11] M. v.d. Silva, C. E. Hori, M. H. M. Reis, *Fluid Phase Equilib.* **2015**, *406*, 168–174.

[12] C. J. Stacy, C. A. Melick, R. A. Cairncross, *Fuel Process. Technol.* **2014**, *124*, 70–77.

[13] S. M. Silva, A. F. Peixoto, C. Freire, *Renewable Energy* **2020**, *146*, 2416–2429.

[14] P. Moradi, M. Saidi, A. T. Najafabadi, *Process Saf. Environ. Prot.* **2021**, *147*, 684–692.

[15] G. Berrebi, P. Dufresne, Y. Jacquier, *Environ. Prog.* **1993**, *12*, 97–100.

[16] C. Carlucci, L. Degennaro, R. Luisi, *Catalysts* **2019**, *9*, 75.

[17] P. Karan, P. Mukhopadhyay, R. Chakraborty, *Asia-Pac. J. Chem. Eng.* **2020**, *15*, e2379.

[18] G. Corro, N. Sánchez, U. Pal, S. Cebada, J. L. G. Fierro, *Appl. Catal. B* **2017**, *203*, 43–52.

[19] N. V. S. Praneeth, S. Paria, *New J. Chem.* **2020**, *44*, 2619–2629.

[20] O. Carp, C. L. Huisman, A. Reller, *Prog. Solid State Chem.* **2004**, *32*, 33–177.

[21] K. Rajeshwar, M. E. Osugi, W. Chanmanee, C. R. Chenthamarakshan, M. V. B. Zanoni, P. Kajitvichyanukul, R. Krishnan-Ayer, *J. Photochem. Photobiol. C* **2008**, *9*, 171–192.

[22] I. K. Konstantinou, T. A. Albanis, *Appl. Catal. B* **2003**, *42*, 319–335.

[23] D. Kanakaraju, B. D. Glass, M. Oelgemöller, *Environ. Chem. Lett.* **2014**, *12*, 27–47.

[24] N. Hoffmann, *Aust. J. Chem.* **2015**, *68*, 1621.

[25] P. P. Wulandari, M. T. Adiwibowo, A. S. Redjeki, M. Ibadurrohman, Slamet, *Asian J. Chem.* **2019**, *31*, 2394–2396.

[26] T. van Gerven, G. Mul, J. Moulijn, A. Stankiewicz, *Chem. Eng. Process.* **2007**, *46*, 781–789.

[27] M. Oelgemöller, N. Hoffmann, O. Shvydkiv, *Aust. J. Chem.* **2014**, *67*, 337.

[28] T. Fukuyama, M. Kasakado, M. Hyodo, I. Ryu, *Photochem. Photobiol. Sci.* **2022**, DOI 10.1007/s43630-021-00151-6.

[29] Y. Mo, K. F. Jensen, *React. Chem. Eng.* **2016**, *1*, 501–507.

[30] M. Motegh, J. R. van Ommen, P. W. Appel, M. T. Kreutzer, *Environ. Sci. Technol.* **2014**, *48*, 1574–1581.

[31] R. Welter, J. Silva Jr., M. de Souza, M. Lopes, O. Taranto, H. Santana, *Preprints* **2022**, 2022020257, DOI 10.20944/preprints202202.0257.v1.

[32] M. Rahimi, F. Mohammadi, M. Basiri, M. A. Parsamoghadam, M. M. Masahi, *J. Inst. Chem.* **2016**, *64*, 203–210.

[33] J. M. Pettibone, D. M. Cwiertny, M. Scherer, V. H. Grassian, *Langmuir* **2008**, *24*, 6659–6667.

[34] J. Maser, *Microsc. Microanal.* **2001**, *7*, 536.

[35] B. M. Craig, *Can. J. Chem.* **1953**, *31*, 499–504.

[36] M. Setvin, X. Shi, J. Hulva, T. Simschitz, G. S. Parkinson, M. Schmid, C. di Valentin, A. Selloni, U. Diebold, *ACS Catal.* **2017**, *7*, 7081–7091.

[37] D. Yang, Y. Li, X. Liu, Y. Cao, Y. Gao, Y. R. Shen, W.-T. Liu, *PNAS* **2018**, *115*, E3888.

[38] G. Li, C. P. Richter, R. L. Milot, L. Cai, C. A. Schmuttenmaer, R. H. Crabtree, G. W. Brudvig, V. S. Batista, *Dalton Trans.* **2009**, *1*, 10078–10085.

[39] Aeroxide, https://products-re.evonik.com/www2/uploads/productfinder/AEROXIDE-TiO2-P-25-EN.pdf (accessed November 12, 2021).

[40] A. Wang, H. Zhang, H. Li, S. Yang, *Adv. Polym. Technol.* **2019**, *2019*, 4041631.

[41] Z. Wu, C. Chen, L. Wang, H. Wan, G. Guan, *Ind. Eng. Chem. Res.* **2016**, *55*, 1833–1842.

[42] F. F. Roman, A. E. Ribeiro, A. Queiroz, G. G. Lenzi, E. S. Chaves, P. Brito, *Fuel* **2019**, *239*, 1231–1239.

[43] S. S. Vieira, Z. M. Magriotis, M. F. Ribeiro, I. Graça, A. Fernandes, J. M. F. M. Lopes, S. M. Coelho, N. A. v. Santos, A. A. Saczk, *Microporous Mesoporous Mater.* **2015**, *201*, 160–168.

[44] S. S. Vieira, Z. M. Magriotis, N. A. V. Santos, A. A. Saczk, C. E. Hori, P. A. Arroyo, *Bioresour. Technol.* **2013**, *133*, 248–255.

[45] F. W. Harun, N. ʻIzzati M. Jihadi, S. Ramli, N. R. A. Hassan, ʻNur ʻAtikah Mat Zubir, *AIP Conf. Proc.* **2018**, *1972*, 030025.

[46] N. Mostafa Marzouk, A. O. Abo El Naga, S. A. Younis, S. A. Shaban, A. M. el Torgoman, F. Y. el Kady, *J. Environ. Chem. Eng.* **2021**, *9*, 105035.

[47] K. P. Flores, J. L. O. Omega, L. K. Cabatingan, A. W. Go, R. C. Agapay, Y. H. Ju, *Renewable Energy* **2019**, *130*, 510–523.

[48] Y. Essamlali, M. Larzek, B. Essaid, M. Zahouily, *Ind. Eng. Chem. Res.* **2017**, *56*, 5821–5832.

[49] A. Patel, V. Brahmkhatri, *Fuel Process. Technol.* **2013**, *113*, 141–149.

[50] M. I. Senoymak Tarakcı, O. Ilgen, *Chem. Eng. Technol.* **2018**, *41*, 845–852.

[51] N. R. M. Sturt, S. S. Vieira, F. C. C. Moura, *J. Environ. Chem. Eng.* **2019**, *7*, 102866.

[52] C. Hong, W. Haiyun, *Bioresour. Technol.* **2010**, *101*, 5487–5493.

[53] S. M. Sidik, S. Triwahyono, A. A. Jalil, Z. A. Majid, N. Salamun, N. B. Talib, T. A. T. Abdullah, *Chem. Eng. J.* **2016**, *295*, 1–10.

[54] J. Bonet, V. Plesu, E. B. Ruiz, P. Iancu, J. Llorens, *Rev. Chim.* **2014**, *65*, 358–361.

[55] A. L. Cardoso, S. C. G. Neves, M. J. da Silva, *Energy Fuels* **2009**, *23*, 1718–1722.

[56] D. Chandler, *Nature* **2002**, *417*, 491–491.

[57] B. Han, F. Yin, S. Liu, X. Zhao, J. Liu, C. Wang, H. Yang, W. Zhang, *Chiang Mai J. Sci.* **2019**, *46*, 714–726.

[58] A. H. Mohammad Fauzi, N. A. Saidina Amin, *Energy Convers. Manage.* **2013**, *76*, 818–827.

[59] L. L. Rade, C. O. T. Lemos, M. A. S. Barrozo, R. M. Ribas, R. S. Monteiro, C. E. Hori, *Renewable Energy* **2018**, *115*, 208–216.

[60] P. Prasertpong, C. Jaroenkhasemmeesuk, J. R. Regalbuto, J. Lipp, N. Tippayawong, *Energy Rep.* **2020**, *6*, 1–9.

[61] R. Foroutan, R. Mohammadi, B. Ramavandi, *Fuel* **2021**, *291*, 120151.

[62] G. Baskar, I. Aberna Ebenezer Selvakumari, R. Aiswarya, *Bioresour. Technol.* **2018**, *250*, 793–798.

[63] N. Ghani, J. Iqbal, S. Sadaf, H. N. Bhatti, M. Asgher, *ChemistrySelect* **2020**, *5*, 9245–9253.

[64] O. I. Micic, Y. Zhang, K. R. Cromack, A. D. Trifunac, M. C. Thurnauer, *J. Phys. Chem.* **1993**, *97*, 7277–7283.

[65] B. Ohtani, *Adv. Inorg. Chem.* **2011**, *63*, 395–430.

[66] F. Narenji-Sani, R. Tayebee, M. Chahkandi, *ACS Omega* **2020**, *5*, 9999–10010.

[67] S. Z. Hassan, M. Vinjamur, *Ind. Eng. Chem. Res.* **2013**, *52*, 1205–1215.

[68] A. Osmont, L. Catoire, I. Gökalp, *Int. J. Chem. Kinet.* **2007**, *39*, 481–491.

[69] M. Lapuerta, J. Rodríguez-Fernández, F. Oliva, *Chem. Phys. Lipids* **2010**, *163*, 172–181.

[70] M. Oelgemöller, *J. Chem. Rev* **2016**, *116*, 9664–9682.

[71] Quantachrome Instruments, **2009**, *05098–4.0*.

[72] H. J. Cho, S. H. Kim, S. W. Hong, Y.-K. Yeo, *Fuel* **2012**, *93*, 373–380.

[73] Z. Hussain, R. Kumar, *Int. J. Green Energy* **2018**, *15*, 629–640.

[74] K. N. Prasanna Rani, T. S. V. Ramana Neeharika, T. P. Kumar, B. Satyavathi, C. Sailu, *J. Oleo Sci.* **2016**, *65*, 441–445.

[75] M. Veillette, A. Giroir-Fendler, N. Faucheux, M. Heitz, *Chem. Eng. J.* **2017**, *308*, 101–109.

[76] I. Ould Brahim, M. Belmedani, H. Hadoun, A. Belgacem, *React. Kinet. Mech. Catal.* **2021**, *133*, 1075–1095.

[77] C. U. Ameh, A. Jimoh, A. S. Abdulkareem, A. J. Otaru, *IOSR-JM* **2013**, *6*, 70–83.

[78] R. Kar, *J. Chem. Eng. Process Technol.* **2012**, *04*, 1000143.

[79] H. R. S. Khezrianjoo, *Chem. Sci.* **2012**, *85*, CSJ85.

[80] K. H. Choo, *Current Trends and Future Developments on (Bio-) Membranes: Photocatalytic Membranes and Photocatalytic Membrane Reactors* **2018**, Elsevier, 297–316.

[81] R. Ezzati, *Iran. J. Catal.* **2018**, *8*, 41–46.

[82] W. Z. Tang, Huren An, *Chemosphere* **1995**, *31*, 4157–4170.

[83] S. Chaemchuen, P. M. Heynderickx, F. Verpoort, *Chem. Eng. J.* **2020**, *394*, 124816.